Materials Today Bio 16 (2022) 100391

Contents lists available at ScienceDirect

Materials Today Bio

journal homepage: www.journals.elsevier.com/materials-today-bio

Mechanosensation mediates volume adaptation of cardiac cells and spheroids in 3D

Ian L. Chin [a], Sebastian E. Amos [a], Ji Hoon Jeong [c,d], Livia Hool [a,b], Yongsung Hwang [c,d], Yu Suk Choi [a,*]

[a] School of Human Sciences, The University of Western Australia, Perth, WA, Australia
[b] Victor Chang Cardiac Research Institute, Sydney, NSW, Australia
[c] Soonchunhyang Institute of Medi-bio Science (SIMS), Soonchunhyang University, Cheonan-si, Chungnam-do, 31151, Republic of Korea
[d] Department of Integrated Biomedical Science, Soonchunhyang University, Asan-si, Chungnam-do, 31538, Republic of Korea

ARTICLE INFO

Keywords:
Mechanobiology
Heart disease
Myocardial infarction
Fibrosis
Cell biomechanics

ABSTRACT

With the adoption of 3-dimensional (3D) cell culture for *in vitro* modelling of cardiac function and regenerative medicine applications, there is an increased need to understand cardiomyocyte mechanosensation in 3D. With existing studies of cardiomyocyte mechanosensation primarily focussed on the behaviour of individual cells in a 2-Dimensional context, it is unclear whether mechanosensation is the same in a 3D, multicellular context. In this study, H9C2 cardiac-derived myoblasts were encapsulated as individual cells and as cell spheroids within stiffness gradient gelatin methacryloyl (GelMA) hydrogels to investigate individual and collective cardiac cell mechanosensation in 3D. Over a 3.68–17.52 kPa stiffness range, it was found that H9C2 cells have a limited capacity to adapt their volume to increasing substrate stiffness, demonstrated by the lack of changes in cell volume and shape across the stiffness gradient. Morphological trends were reflected by the expression of the mechanomarkers YAP, MRTF-A and Lamin-A, which were better correlated with cell and nuclear volume than with substrate stiffness. The localisation of YAP and MRTF-A were dependent on the relative volumes of the cytoplasm and nucleus while Lamin-A expression was elevated with increasing cytoplasmic and nuclear volumes. When cultured as spheroids rather than as individual cells, H9C2 cells adopted a distinct morphology with comparably smaller nuclei than individually cultured cells, while retaining the same overall cell volume. As spheroids, H9C2 cells were sensitive to stiffness cues, shown by decreasing YAP and MRTF-A nuclear localisation, increasing Lamin-A expression, and increasing vinculin expression with increasing substrate stiffness. Like the individually cultured H9C2 cells, mechanomarker expression was correlated to volume adaptation. With increasing cytoplasmic volume, YAP and MRTF-A became less nuclear localised, vinculin expression was increased, and with increasing nuclear volume, the Lamin-A expression fincreased. Together, these data suggest that cardiac cell volume adaptation may be enhanced by cell-cell interactions.

1. Introduction

In emulating the developing, healthy, and infarcted hearts, the changes in tissue mechanics are a key element to consider. The most marked long-term change is the rapid deposition of a disorganised collagen scar [1–3] that is potentially three-times stiffer than a healthy myocardium [4]. It has been established within a 2D context that cardiomyocytes can sense and respond to a variety of mechanical cues from the extracellular matrix (ECM), such as stiffness [5–9] and topography [10].

Many of these above studies have focused on functional elements, such as how stiffness changes affect cardiomyocyte contractility [5,6,11] or how different microenvironments affect cardiomyocyte maturation [7,8,12]. However, the focus of these aforementioned studies has been on single-cell cardiomyocyte dynamics and was often limited to 2D microenvironments.

Within the cardiac space, 3D cell cultures are being used to develop *in-vivo* models of cardiac function [13] and 3D printed cardiac constructs for regenerative medicine applications [14,15]. These platforms have shown that cell-cell interactions are a crucial element of cardiac construct

* Corresponding author. School of Human Sciences, The University of Western Australia, 35 Stirling Highway, Crawley, WA, 6009, Australia.
E-mail address: yusuk.choi@uwa.edu.au (Y.S. Choi).

https://doi.org/10.1016/j.mtbio.2022.100391
Received 9 May 2022; Received in revised form 2 August 2022; Accepted 2 August 2022
Available online 13 August 2022

design, providing greater cardiomyocyte maturation and cell survival *in-vitro* [16–18].

It is unclear what impact cell-cell signalling has on cardiac mechanosensation within these biomimetic platforms. Great strides have been made using mesenchymal cells to unpack the mechanisms behind mechanosensation in 3D [19–21], which have illustrated that cells respond very differently to 3-Dimensional (3D) microenvironments compared to an equivalent 2-Dimensional (2D) microenvironment. In 3D cell culture, volume adaptation, a cell's capacity to adapt its volume within a 3D space, has recently been found to be a major determinant of mechanosensation [19,21,22]. In a 2D microenvironment, cells can adapt their volume in a less restricted fashion (e.g. cell spreading on 2D tissue culture plastic) whereas cell volume is constrained by surrounding 3D microenvironment. In 3D, cell volume is determined by a cell's capacity to remodel [22] and degrade the surrounding ECM [19]. The expression of canonical markers of mechanosensation such as YAP, MRTF-A and Lamin-A have strongly been correlated with cell volume in 3D [19,21,22]. It has been hypothesised that restricted cell volume impairs a cell's capacity to generate traction forces and, in turn, respond to mechanical cues from the ECM [21]. Volume adaptation in cardiomyocytes has not been characterised and it is unknown whether cardiomyocyte volume adaptation is influenced by cell-cell interactions.

In this study, we employ a versatile Gelatin Methacryloyl (GelMA) based cell culture platform to explore the mechanosensation of cardiomyocytes in a 3D microenvironment. With this platform, we exposed H9C2 cells, cultured as individual cells and in spheroid culture, to a physiological range of stiffnesses over a continuous stiffness gradient and observed how 3D volume adaptation of H9C2 governs mechanosensitive responses of YAP, MRTF-A and Lamin-A. Our work provides a simple approach to characterising the mechanosensation of individual cardiac cells and groups of cardiac cells in a 3D microenvironment.

2. Methods

2.1. Hydrogel fabrication and cell encapsulation

GelMA hydrogels were prepared based on a previously described method [21,23,24]. In brief, a mould was constructed by 3D-printing a resin structure with a 12 × 12 × 0.5 mm^3 empty space in the centre. This structure was glued to a glass slide, creating a 12 × 12 × 0.5 mm^3 reservoir with a transparent underside. To create the linear stiffness gradient, a photomask with a 20–100% light transmittance gradient was applied to the underside of the mould to allow for variable photopolymerization of GelMA based on UV light transmittance through the photomask (Fig. 1A).

A precursor solution was made by dissolving lyophilized GelMA in phosphate buffered saline (PBS; Gibco) with Irgacure 2959 photoinitiator (Sigma) in 70% ethanol was added to the precursor solution to achieve a final concentration of 90 mg/ml of GelMA and was 1 μg/ml of photoinitiator. GelMA was dissolved in a 37 °C water bath for 1 h before being stored at 4 °C for use the next day.

On the day of hydrogel fabrication, methacrylated coverslips were prepared. Glass coverslips (15 × 15 mm^2; Menzel-Gläser) were cleaned in a UV ozone cleaner (Bioforce Nanosciences UV/Ozone ProCleaner) for 1 min on each side. Coverslips were then immersed in a solution containing ethanol (96.5% V/V), 3-(trimethoxysilyl)propyl methacrylate (0.5% V/V) (Merk), and glacial acetic acid (3% V/V) for 5 min before being rinsed in pure ethanol. Coverslips were dried in the air before use. The moulds were coated in Dichlorodimethylsilane (Sigma) to prevent the hydrogel from sticking to the mould when set. While preparing methacrylated coverslips and moulds, the GelMA precursor solution was warmed to 37 °C in a water bath for 1 h.

For encapsulation of individual cells, H9C2 cells were resuspended in GelMA (1.1 × 10^5 H9C2 cells per hydrogel; 8.55 cells/μl). Cell-laden GelMA was then carefully pipetted into the moulds and covered with a methacrylated coverslip. Cell-laden GelMA was exposed to UV light (360 nm, 3.6 mW/cm^2) for 130 s before the hydrogels were retrieved from the mould and placed in a 12-well plate for cell culture (Fig. 1A). Cells were maintained in growth media (10% FBS, 1% antibiotic and antimycotic, and 89% DMEM), changed every three days for 10 days before being fixed and stained.

For experiments using H9C2 spheroids, cell spheroids were formed using AggreWell 400 (Stem Cell) microwell system. As per the manufacturer's instructions, wells were coated in an anti-adherence medium (Stem Cell) for 30 min before being washed 3x with warm media. Cells in suspension were added to each well to achieve a density of 50, 100 and 200 cells per microwell, representing small, medium and large spheroids. The cells were left in the AggreWells overnight to settle into the microwells before being harvested the next day via gentle aspiration and resuspended in GelMA. GelMA was prepared as described above and the same conditions were used to set the hydrogels. As above, cell spheroids were maintained for 10 days before being fixed and stained.

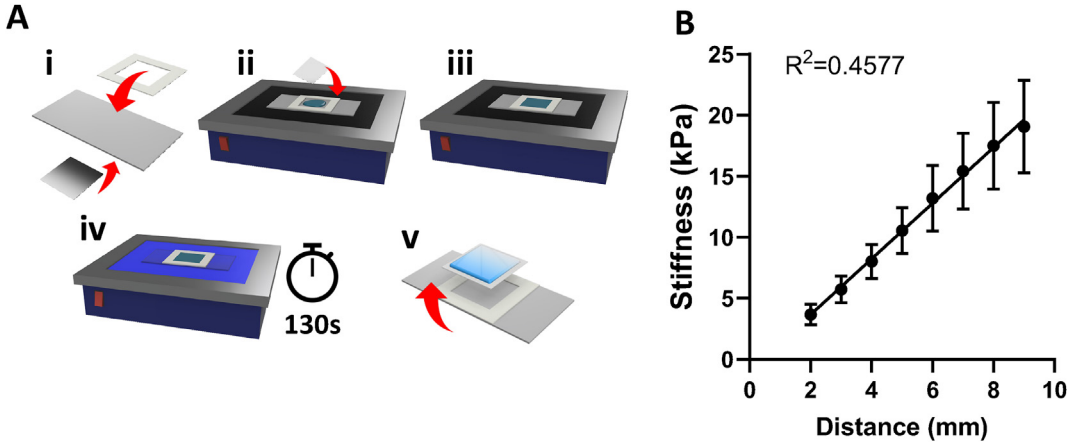

Fig. 1. Fabrication of stiffness gradient GelMA hydrogels. **A. i)** A mould was made by attaching a 3D printed resin structure to glass slide, forming a 12 × 12 × 0.5 mm^3 reservoir. A gradient photomask was attached to the bottom of the slide, under the reservoir. **ii)** The reservoir in the mould was filled with cell-laden GelMA and **iii)** covered with a methacrylate-coated coverslip. **iv)** Cell laden GelMA was photopolymerized with UV light (360 nm) for 130s and then **v)** carefully removed from the mould. **B.** Atomic force microscopy was used to measure Young's elastic moduli across an 8 mm band running along the same axis as the photomask's gradient. A stiffness range of 3.68–19.08 kPa was detected, giving a linear stiffness gradient of 2.28 kPa mm^{-1} (Linear Regression, $R^2 = 0.9968$, $P < 0.05$, $n = 6$).

2.2. Atomic force microscopy

To measure the stiffness that cells would be exposed to, we measured Young's compressive moduli of cell-free hydrogels produced at the same time and under the same conditions as the cell-laden hydrogels. Stiffness was measured using an MFP-3D atomic force microscope (Asylum Research) using 200 μm Chromium/gold-coated pyrex-nitride cantilevers with triangular-shaped tips (NanoWorld model PNP-TR). Hydrogels immersed in PBS were probed with 2 nN indentations at an approach velocity of 2 μm/s and with a retraction velocity of 10 μm/s. Each indentation was made in triplicate to ensure that the reading was stable. All measurements were taken at 24.5 °C to control for temperature dependent changes to measured stiffness [25]. As previously described, custom-written code in Igor Pro was used to determine Young's modulus from the linear portion of contact generated force curves [26].

Eight indentations were made at 1 mm intervals along the axis of the stiffness gradient, beginning 2 mm away from the softest edge and moving towards the stiffest edge. Indentations were made on three hydrogels per biological replicate and averaged to give an estimate of the stiffness at a given displacement from the edge of the hydrogel.

2.3. Immunocytochemistry

As a measure of mechanosensation, individually cultured cells were stained for either YAP, MRTF-A or Lamin-A. For spheroid culture, samples were stained for Vinculin in addition to YAP, MRTF-A and Lamin-A. All immunofluorescent staining cells were fixed in paraformaldehyde (4% in PBS) for 30 min and washed with PBS (three times for 5-min each). The cells were then permeabilized in Triton X-100 (1% in PBS) for 30 min and washed with PBS (three times for 5-min each). Primary antibodies for YAP (sc-101199, Santa Cruz), MRTF-A (sc-390,324, Santa Cruz) and Vinculin (ab129002, Abcam) were diluted 1:100 in BSA (2% in PBS) and incubated on samples for 72-h at room temperature, followed by rinsing with PBS (three-times for 20-min each). A secondary antibody solution was prepared, containing BSA, Rhodamine Phalloidin (R415, Invitrogen; diluted to 1:200), and Alexafluor-488 (Anti-mouse (ab150113, Abcam) for YAP and MRTF-A, Anti-Rabbit (ab150077, Abcam) for Vinculin; diluted to 1:200), and was incubated with YAP, MRTF-A and Vinculin stained samples respectively for 2-h at 37 °C before being rinsed-off with PBS (three-times for 20-min each). A pre-conjugated Lamin-A antibody (ab205769, Abcam) was diluted to 1:300 in BSA and was incubated on samples alongside Rhodamine Phalloidin diluted to 1:200 in BSA for 2 h at 37 °C before samples were rinsed with PBS (three-times for 20-min each). Finally, all samples were stained with DAPI (D9542, Sigma Aldrich) diluted to 1:400 in PBS for 30 min at room temperature before being washed with PBS (three times for 20-min each). Samples were mounted with Diamond Slow fade (Life Technologies) and stored at 4 °C until imaged with confocal microscopy.

2.4. Confocal microscopy

Images of individual cell cultures were captured on a Nikon C2+ confocal microscope using NIS-Elements Advanced Software (Nikon). A 20× air objective was used to capture a Z-series of images at a pixel resolution of 1024 × 1024 pixels and in 4 μm steps. Images of spheroids were captured on a Nikon A1R Confocal Microscope using NIS-Elements Advanced Software (Nikon). A 20× air objective was used to capture images at a pixel resolution of 1024 × 1024 and in 1.5 μm steps. For all conditions, images were captured every 1 mm over an 8 mm span along the stiffness gradient, starting 2 mm away from the softest edge of the hydrogel. The span where images were captured was matched to the span where AFM indentations were taken so that the stiffness at each image location could be estimated based on the distance from the edge of the hydrogel.

2.5. Image analysis

Image analysis was performed in ImageJ/FIJI with additional processing and analysis plugins installed. All images within a given dataset were acquired and processed with identical camera, device, and analysis settings. Pre-processing of single-cell and spheroid images was done with CLIJ2 to generate the appropriate precursors for nuclei segmentation [27,28]. Briefly, images were denoised with Gaussian Blur 3D, then an inverted mask, labelled 3D point maxima (box), and a greater constant threshold were created. These images were fed into MorpholibJ's marker-controlled watershed to segment and uniquely identify each nucleus in both individual cell and spheroid datasets [29]. Randomly selected images were used to optimise segmentation parameters for each grouped dataset with the CLIJx-Assistant prior to batch analysis of images. The same approach was employed to segment the single-cell volumes. Cell objects that were touching the borders of the image were removed. To relate a cell object to its corresponding nucleus, cell label numbers were reduced to one and then multiplied by the nuclear object image, so that cell volumes were assigned the same object identification number. The image calculator was also used to subtract the nuclei objects from the cell volume segmentation, thus creating a cytoplasmic region of interest (ROI). For spheroid analysis, the nuclei objects were subtracted from the whole spheroid threshold to create a cytoplasmic volume. The generated ROIs were then used to quantify the integrated density of fluorescent stains of interest.

For YAP and MRTF-A, the level of nuclear localisation was derived from the total intensity values measured as follows:

$$Nuc \Big/ Cyt = \frac{Nuclear\ Intensity}{Cytoplasmic\ Intensity}$$

The volume of cells within a spheroid was estimated as follows:

$$Cell\ Volume = \frac{Total\ Spheroid\ Volume}{Number\ of\ Nuclei}$$

2.6. Statistical analysis

All statistical analysis was performed in GraphPad Prism. Pearson's correlation coefficient was used to identify relationships between stiffness, volume, and their respective dependent variables. Two-way ANOVA were performed to compare spheroid- and individually-cultured cell morphologies, followed by Šídák's multiple comparisons test where a significant difference was detected. A minimum of three biological replicates were analysed for each experiment.

3. Results and discussion

3.1. Photopolymerized GelMA is an effective method of producing stiffness gradient hydrogels

Photopolymerization of GelMA was an effective method for producing linear stiffness gradients (Fig. 1A). Our method, detailed in our past studies [21,23], uses a photomask to variably block UV light across the hydrogel to spatially control the degree of polymerization across the hydrogel; as more light is transmitted through the photomask, the stiffer the hydrogel becomes. Under the conditions we used, we measured a 2.28 kPa/mm stiffness gradient through atomic force microscopy, giving us an effective stiffness range from 3.68 kPa to 19.08 kPa (Fig. 1B). In our past characterisations of GelMA, we have found that stiffness measured from surface indentations is representative of the stiffness measured within the bulk of the hydrogel [21,30]. In our past characterisations of GelMA, we have found that stiffness measured from surface indentations is representative of the stiffness measured within the bulk of the hydrogel [21,30]. Using optical coherence microscopy, we found that the stiffness

gradient was measurable at 500 μm in the Z axis (halfway within a 1 mm thick GelMA hydrogel).

We have previously observed H9C2 cells being responsive to this stiffness range on 2D hydrogels, where we found that with increasing stiffness cell size increased by 44% and nuclear YAP localisation increased by 37% [9].

3.2. Individual H9C2 cells have a limited capacity to expand in 3D GelMA

Over the course of 10 days of culture, we found limited changes in cell morphology with increasing stiffness. We found that individually encapsulated H9C2 cells displayed the same spreading at all stiffnesses, typically adopting a round shape with small projections (Fig. 2A). Cell volume, cell surface area and cell sphericity (Fig. 2B–D), did not change significantly over the stiffness gradient. No trends were observed in nuclear volume and surface area (Fig. 2E and F) although nuclei became less spherical as stiffness increased (Fig. 2G). We did not find any relationship between stiffness and YAP and MRTF-A localisation or stiffness and Lamin-A expression (Fig. 3).

These results are consistent with previous 3D studies, which found that trends in the expression of mechanomarkers are better correlated with cell volumes rather than substrate stiffness [19–21]. To investigate the correlation in H9C2 cells, we pooled all the data across the whole stiffness gradient and compared mechanomarker expression to the cell and nuclear volume of the respective cell (Fig. 4). Cells with greater cytoplasmic volume tended to have more cytoplasmic localised YAP and MRTF-A (Fig. 4G and H), however, cells with larger nuclei tended to have greater nuclear localisation of YAP and MRTF-A (Fig. 4J and K). Lamin-A expression increased with both nucleus and cell size (Fig. 4I, L), as observed in the past [21].

Conventionally, it is agreed that when cells are mechanically stimulated, YAP [31] and MRTF-A [32,33] translocate into the nucleus and Lamin-A is expressed at greater levels in the nuclear lamina [26,34]. In 2D cell culture, cells can expand freely and can generate traction forces

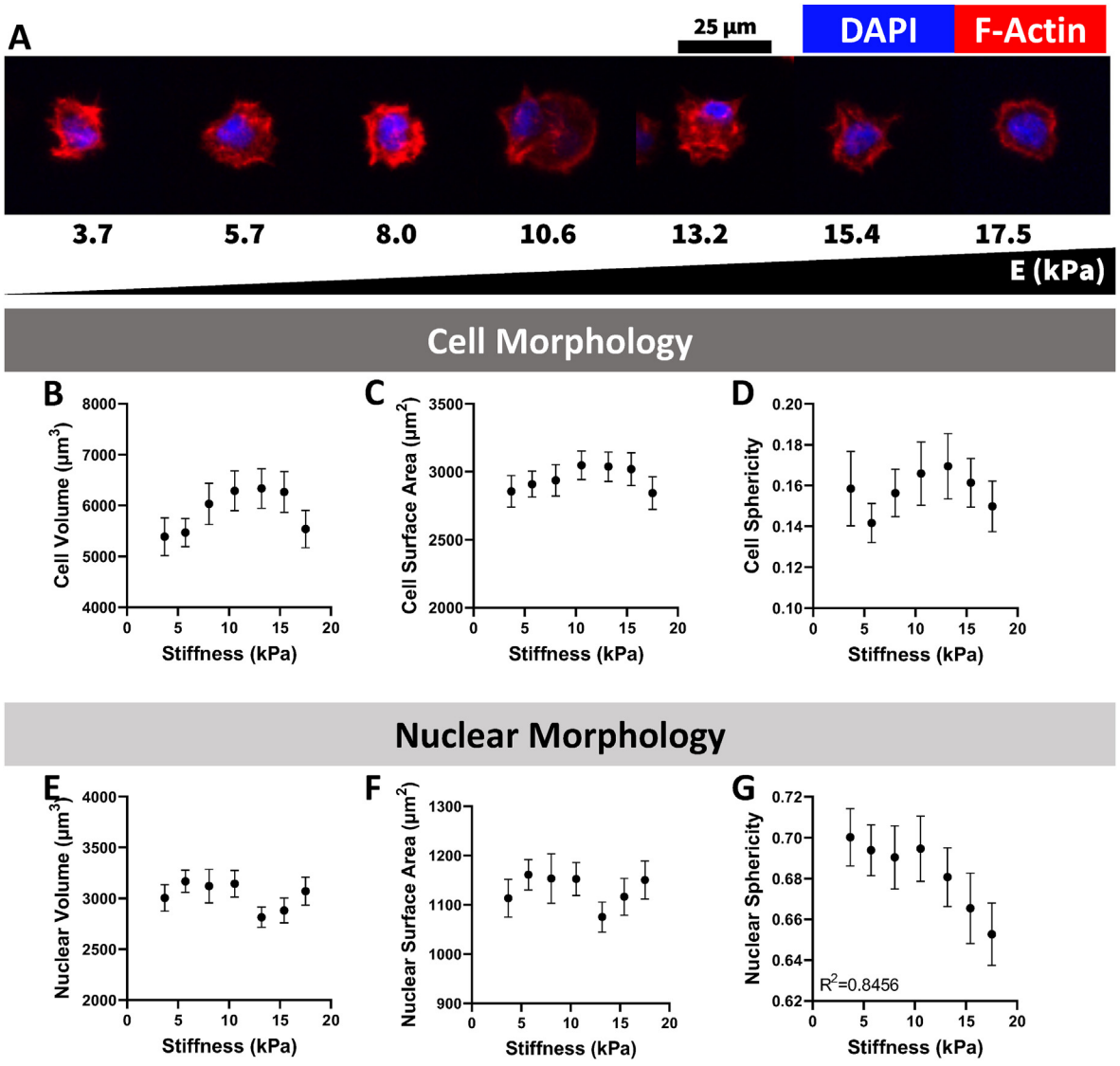

Fig. 2. Morphology of Individual 3D encapsulated H9C2 Cells. **A.** Representative images of H9C2 cells across the stiffness gradient after 10 days of cell culture. Nuclei are visualised with DAPI and F-Actin has been stained to show the cytoplasm. Substrate stiffness was not correlated with **B.** cell volume (Pearson's Correlation, $R^2 = 0.19$, $P > 0.05$, $n = 117$ cells, $N = 3$), **C.** cell surface area (Pearson's Correlation, $R^2 = 0.07$, $P > 0.05$, $n = 117$ cells, $N = 3$) or **D.** cell sphericity (Pearson's Correlation, $R^2 = 0.06$, $P > 0.05$, $n = 104$ cells, $N = 3$). Substrate stiffness was not correlated with **E.** nuclear volume (Pearson's Correlation, $R^2 = 0.17$, $P > 0.05$, $n = 117$ cells, $N = 3$) **F.** nuclear surface area (Pearson's Correlation, $R^2 = 0.03$, $P > 0.05$, $n = 117$ cells, $N = 3$). **G.** Substrate stiffness is negatively correlated with nuclear sphericity (Pearson's Correlation, $R^2 = 0.85$, $P < 0.05$, $n = 104$ cells, $N = 3$). 'n' represents the minimum number of cells measured per stiffnesss, 'N' represents the number of biological replicates. Graphs show mean ± SEM.

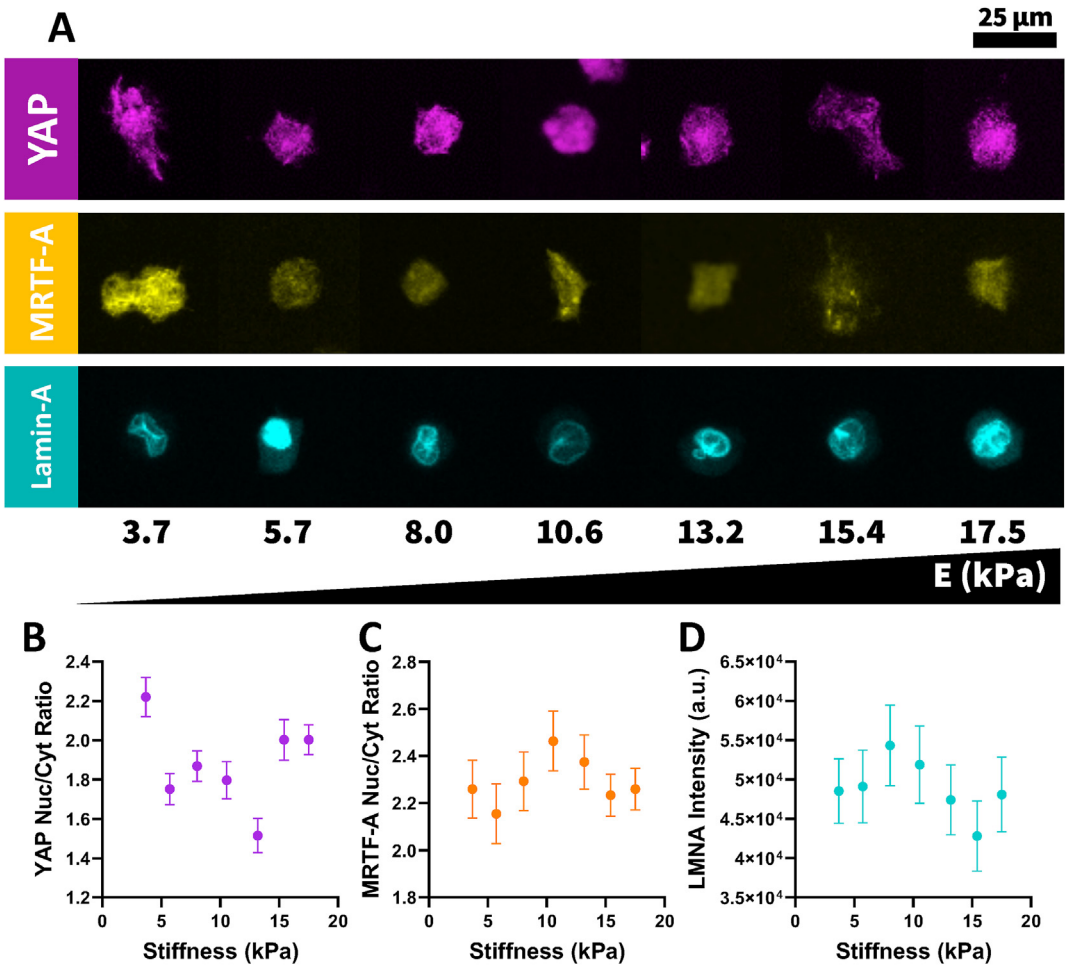

Fig. 3. Mechanomarker expression is not correlated with stiffness in individual cells. **A.** Substrate stiffness was compared against the nuc/cyt ratio of YAP, the nuc/cyt ratio of MRTF-A and the total nuclear intensity of Lamin-A. Representative images of YAP, MRTF-A and Lamin-A in 3D-encapsulated H9C2 cells. Stiffness was not correlated with **B.** YAP localisation (Pearson's Correlation $R^2 = 0.03$, $P > 0.05$, n = 117 cells, N = 3), **C.** MRTF-A localisation (Pearson's Correlation $R^2 = 0.34$, $P > 0.05$, n = 76 cells, N = 3) and **D.** total Lamin-A intensity (Pearson's Correlation $R^2 = 0.22$, $P > 0.04$, n = 141 cells, N = 3). Nuc/Cyt ratios calculated as the $\frac{Total\ Nuclear\ Intensity}{Total\ Cytoplasmic\ Intensity}$. 'n' represents the minimum number of cells measured per stiffnesss, 'N' represents the number of biological replicates. Graphs show mean ± SEM.

proportional to the stiffness of their substrate [19,21]. In a 3D cell culture, the ECM network presents a restriction challenge for cells to overcome. Past studies concluded that a cell's capacity to generate traction forces in 3D depends on its capacity to remodel its microenvironment [19,22]. As such, the activity of mechanosensitive proteins, such as YAP, MRTF-A and Lamin-A, is determined by the cell's capacity to spread and expand within the 3D space more than by the stiffness of a surrounding hydrogel [20,21]. These studies suggested that matrices that were easier to manipulate, such as softer, degradable or viscoelastic matrices, allowed cells to expand and generate greater actin-mediated traction forces, whereas matrices that were difficult for cells to remodel impaired traction force generation, as reflected by YAP localisation [19,21,22]. Conversely, when actomyosin activity was inhibited, cell volumes were reduced and the expression of the mechanomarker Lamin-A responded accordingly [21]. Our results suggest that H9C2 cells have a limited capacity to adapt to or manipulate their surroundings in a 3D context, as illustrated by the lack of variation in cell spreading and shape. Volume mediated trends do suggest that the H9C2 cells can respond to mechanical cues in 3D, however, this is limited by their capacity to expand.

3.3. H9C2 cells are phenotypically different in spheroid culture compared to individual cell culture

In our individual cell culture, we observed few differences in mechanomarker expression between the soft and stiff end of the hydrogel owing to the H9C2 cells limited capacity to spread in 3D hydrogels. One conclusion is that even the 3.68 kPa substrate was too restrictive for the H9C2 cells to overcome, but we also noted that the cells lacked much of the cell-cell interactions they would typically have in a 2D microenvironment [5,9] or *in vivo* [35,36]. It is possible that 3D encapsulation of the H9C2 cells significantly restricted traditional avenues of cell-cell interaction found in a conventional 2D *in-vitro* culture, such as cell migration and cell proliferation. Cell-cell interconnectivity is essential for normal cardiac tissue function, particularly in transmitting mechanical and electric signals between cells [36], and therefore it is possible that a lack of cell-cell interaction contributed to poor volume expansion.

To overcome the lack of cell-cell contact, we formed H9C2 spheroids to ensure cell-to-cell interaction among cells that were encapsulated as spheroids within 3D microenvironment (Fig. 5A). Although there were no observable differences in morphology driven by stiffness, we found that the phenotype of the cells within the spheroid was different to that of individually cultured cells. Total spheroid volume and cytoplasmic volume did not change with stiffness (Fig. 5B and C), although the spheroid surface area did appear to decrease with increasing stiffness (Fig. 5D). Total nuclear volume did not change significantly with increasing stiffness (Fig. 5E).

When we compared individually cultured cells, cells in spheroid culture adopted a distinctly different morphology (Fig. 6A). Like the

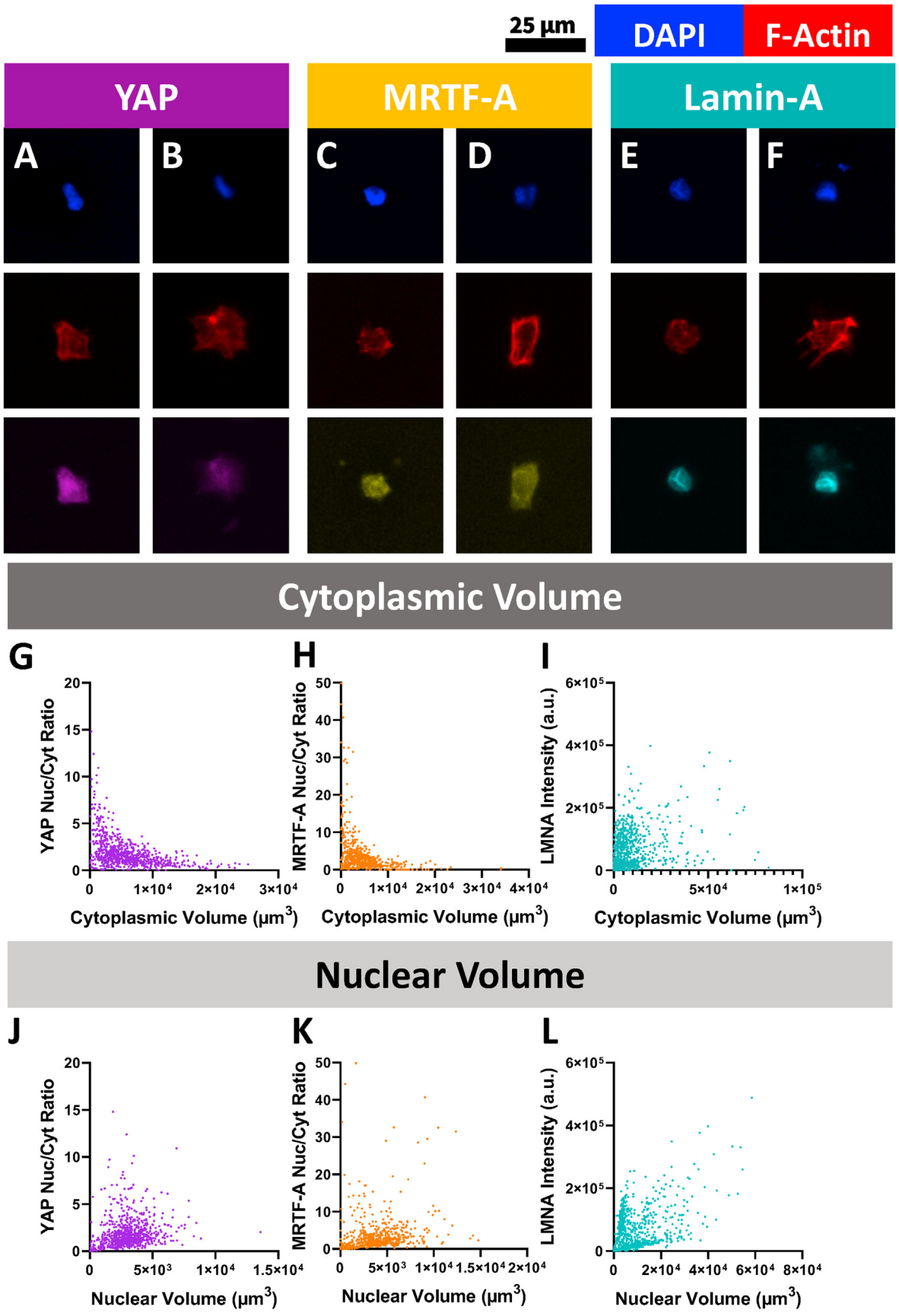

(caption on next page)

Fig. 4. Mechanomarker expression in individual cells correlated with volume. Representative images of small and large cells stained for **A., B.** YAP, **C., D.** MRTFA and **E., F.** Lamin-A. Smaller examples are shown on the left (**A., C.** and **E.**) and larger examples are shown on the right (**B., D.** and **F.**). The cytoplasmic volume of the cells was weakly correlated with **G.** cytoplasmic YAP localisation (Pearson's Correlation, $R^2 = 0.17$, $P < 0.05$, $n = 864$ cells, $N = 3$), **H.** cytoplasmic localisation of MRTF-A (Pearson's Correlation, $R^2 = 0.07$, $P < 0.05$, $n = 649$ cells, $N = 3$) **I.** but was not correlated with the expression of Lamin-A (Pearson's Correlation, $R^2 = 1.24 \times 10\text{-}5$, $P > 0.05$, $n = 1139$ cells, $N = 3$). Weak correlations were observed between nuclear volume and **J.** nuclear YAP localisation (Pearson's Correlation $R^2 = 0.02$, $P < 0.05$, $n = 864$ cells, $N = 3$), **K.** nuclear MRTF-A localisation and nuclear size (Pearson's Correlation $R^2 = 0.01$, $P < 0.05$, $n = 649$ cells, $N = 3$) and **L.** the expression of Lamin-A (Pearson's Correlation, $R^2 = 0.28$, $P < 0.05$, $n = 1149$ cells, $N = 3$). Graphs show individual cells, drawn from three independent biological replicates; 'n' represents the total number of cells analysed.

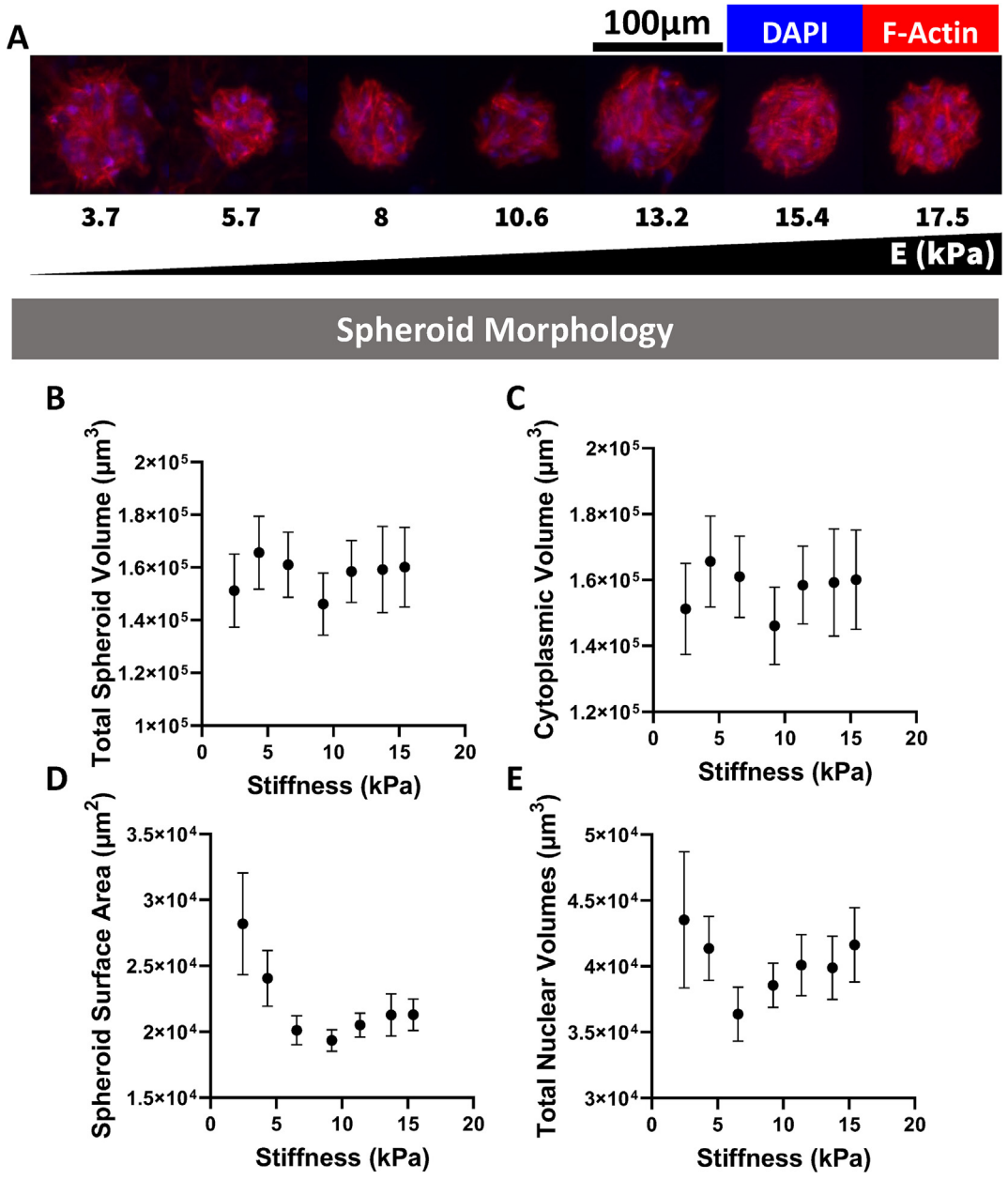

Fig. 5. Morphology of H9C2 cell spheroids. **A.** Representative images of H9C2 spheroids after 10 days of culture across the stiffness gradient. **B.** Total spheroid volume did not change significantly with increasing stiffness (Pearson's Correlation, $R^2 = 0.001$, $P > 0.05$, $n = 26$ spheroids, $N = 3$) and **C.** neither did cytoplasmic volume (Pearson's Correlation, $R^2 = 0.01$, $P > 0.05$, $n = 26$ spheroids, $N = 3$). **D.** Spheroid surface area decreased rapidly between 3.68 kPa and 8.03 kPa (Linear Regression, $R^2 = 0.05$, $P < 0.05$, $n = 26$ spheroids, $N = 3$) before plateauing with increasing stiffness. **E.** Nuclear volume (the sum of volumes of individual nuclei) did not change significantly with increasing stiffness (Pearson's Correlation $R^2 = 0.02$, $P > 0.005$, $n = 26$ spheroids, $N = 3$). 'n' represents the minimum number of spheroids analysed per stiffness and 'N' represents the number of biological replicates. Graphs show mean ± SEM.

individually cultured cells, the volume of single spheroid cells and nuclei within the spheroid remained constant with changes in stiffness (Fig. 6C–E). Cell and the cytoplasmic volume of single cells within the spheroid were comparable to the individually cultured cells (Fig. 6C and D). However, the nuclei of spheroid cultured cells were significantly smaller (Fig. 6E) despite the overall cell volume being largely the same. We calculated the nuclear volume as a percentage of cell volume of single cells in either spheroid or individual cell culture and found that in

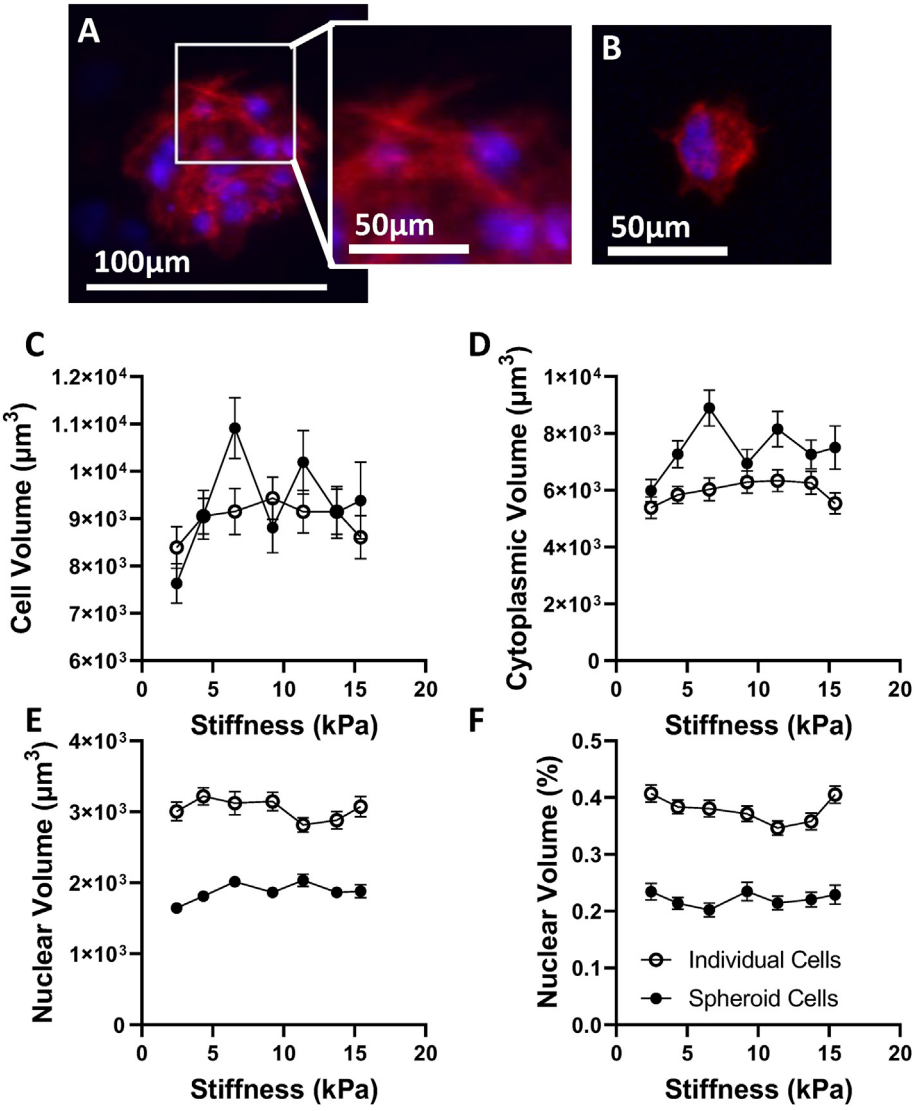

Fig. 6. Cells in spheroid culture have greater cytoplasmic volume than individual cells. **A.** Spheroid-culture cells appear to have more aligned stress fibres greater cytoplasmic volume compared to **B.** individually cultured cells. **C.** Cell volume of individual cells within the spheroid was comparable to individually cultured cells (Two-way ANOVA $P > 0.05$, $n = 117$ cells, $n = 26$ spheroids, $N = 3$). **D.** Cytoplasmic volumes were similar in spheroid culture and individual culture, with cells in spheroid culture having greater cytoplasmic volume at 8.03 kPa (Two-way ANOVA with multiple comparisons, $P < 0.05$, $n = 117$ cells, $n = 26$ spheroids, $N = 3$). **E.** At all stiffnesses, nuclear volume was smaller in spheroid cultured cells compared to individually cultured cells (Two-way ANOVA, Multiple Comparisons $P < 0.05$, $n = 117$ cells, $n = 26$ spheroids, $N = 3$) and similarly **F.** the nuclei in spheroid-cultured cells occupied a smaller percentage of the total cell volume in spheroid culture compared to individual cell culture (Two-way ANOVA, Multiple Comparisons $P < 0.05$, $n = 117$ cells, $n = 26$ spheroids, $N = 3$). 'n' represents the minimum number of cells and spheroids respectively analysed per stiffness. Graphs show mean ± SEM.

spheroid culture the nuclei only occupied 22 ± 0.4% SEM of the cell volume compared to 38 ± 0.9% in individual cell culture (Fig. 6F).

3.4. Mechanomarker expression spheroid culture is guided by substrate stiffness and spheroid volume

When considering spheroids as a whole again, we found weak correlations between stiffness and MRTF-A localisation, Lamin-A and Vinculin expression (Fig. 7). A brief analysis of fluorescent intensities across the X- and Y-axis of spheroids did not indicate differences from the core to the periphery (Fig. S1). With increasing stiffness, MRTF-A appears to become increasingly localised to the cytoplasm (Fig. 7C), Lamin-A expression increases (Fig. 7D) and Vinculin expression also appears to increase (Fig. 7E). These trends are the opposite of what we have observed in 2D [9], similar to what others have found in 3D cell culture [19,21,22]. These studies found that the stiffness-based trends in mechanomarker expression appeared to be the inverse of what is observed in 2D cell culture [19,21] and particularly the localisation of MRTF-A and the expression of Lamin-A appear to be the inverse of what was observed in our 2D study of H9C2 mechanosensation [9]. It has been suggested that Lamin-A provides structural integrity to the nucleus, particularly under strain [37]. MRTF-A is believed to play an important role in cardiac development [38] and in the regulation of actin and intercalated disks in cardiomyocytes under mechanical stress [39]. In our study, increasing substrate stiffness may act as a mechanical stress to the cells, potentially through confinement, mechanical forces exerted by neighbouring cells or some combination of both.

Like the individual-cell culture, we found stronger correlations between mechanomarker expression and spheroid volume rather than with substrate stiffness (Fig. 8). With increasing spheroid volume, there was increasing cytoplasmic localisation of YAP (Fig. 8I) and MRTF-A (Fig. 8J), as indicated by the reduction in the Nuc/Cyt ratio for YAP and MRTF-A, respectively. There was no correlation between YAP localisation (Fig. 8M), MRTF-A localisation (Fig. 8N) and nuclear volume. Lamin-A expression and vinculin expression increased with both total spheroid volume (Fig. 8K and L) and total nuclear volume (Fig. 8O, P), although Vinculin expression lacked the distinct puncta (Fig. 8D, H) normally associated with focal adhesion clustering that is traditionally observed in 2D studies [5,6] and can be found in 3D under certain circumstances [40]. The relationships between nuclear volume, cell volume and mechanomarker expression indicate that the underlying mechanisms of mechanosensation are likely the same in both single-cell and spheroid culture, however the differences in nuclear and cell morphology and the expression of mechanomarkers in response to stiffness illustrate the

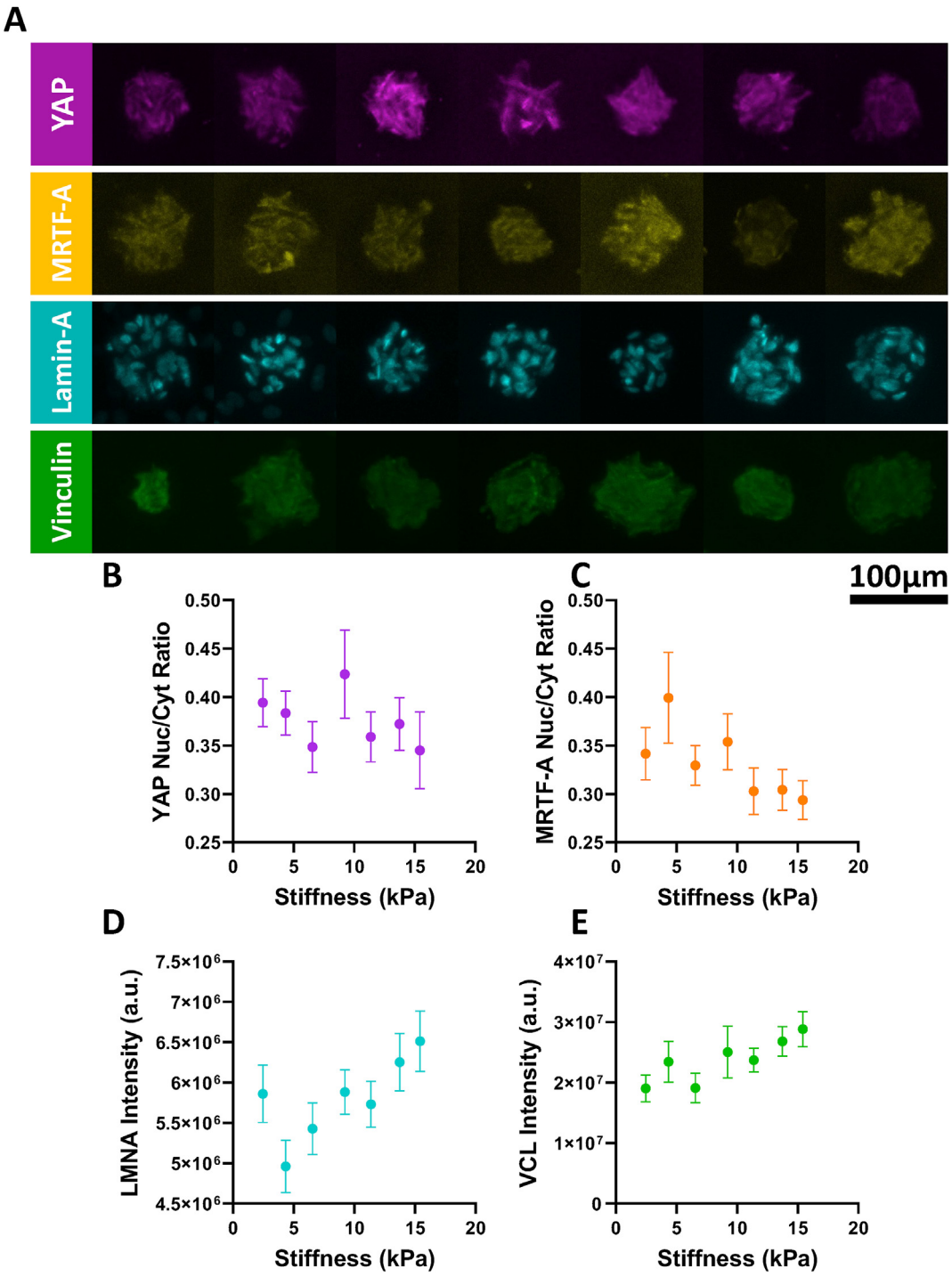

Fig. 7. Mechanomarker expression is weakly correlated with changes in substrate stiffness. Representative images of **A.** YAP localisation, MRTF-A localisation, Lamin-A Expression and Vinculin expression. **B.** There is no significant correlation between stiffness and YAP Nuc/Cyt ratio (Pearson's Correlation, $R^2 = 0.17$, $P > 0.05$, $n = 26$ spheroids, $N = 3$). **C.** Increasing stiffness is correlated with reductions the MRTF-A Nuc/Cyt ratio (Pearson's correlation, $R^2 = 0.58$, $P < 0.05$, $n = 27$ spheroids, $N = 3$). **D.** There is a nonsignificant positive correlation between Lamin-A intensity and stiffness (Pearson's correlation, $R^2 = 0.55$, $P = 0.056$, $n = 31$ spheroids, $N = 3$). **E.** Increasing stiffness is positively correlated with increasing Vinculin intensity (Pearson's correlation, $R^2 = 0.73$, $P < 0.05$, $n = 18$ spheroids $N = 3$). 'n' represents the minimum number of speroids analysed per stiffness, 'N' represents the number of biological replicates. Graphs show mean ± SEM.

significant functional impact cell-cell contact can have on cell phenotype: while there were no distinct trends in mechanomarker expression with stiffness in single-cell culture, there were significant trends in mechanomarker expression in spheroid culture despite mechanomarker expression being seemingly volume mediated in both cases. Our results follow the same trends as previous studies, which suggested mechanosensation is driven by actomyosin activity [22]. We felt this was a fitting explanation for our results as our cell spheroids, which had significantly greater cytoplasm (proportional to the total cell volume) than the individual cells, were more mechanically sensitive than the individual cells, as shown by the expression of the mechanomarkers YAP, MRTF-A and Lamin-A.

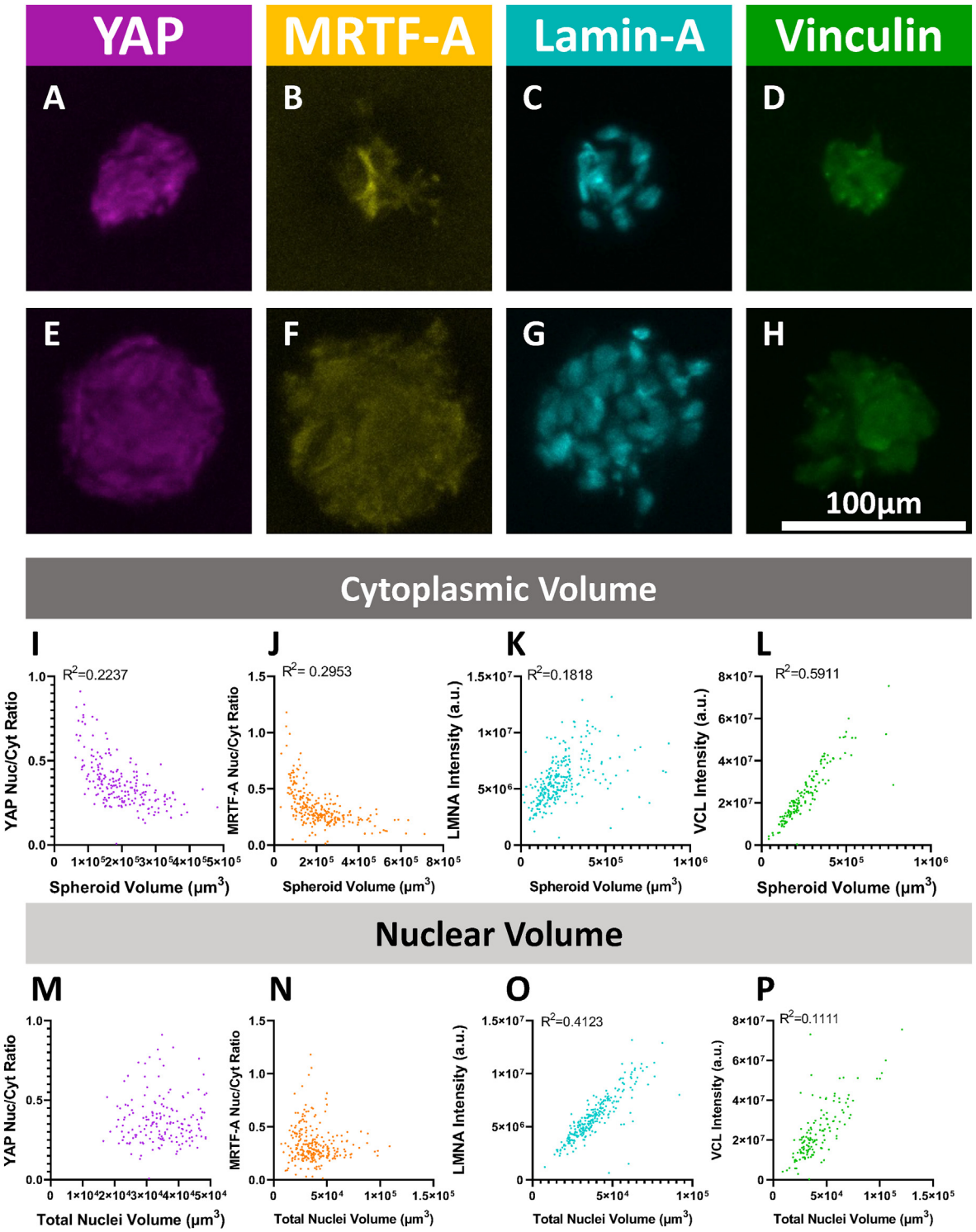

Fig. 8. Mechanomarker expression correlates with spheroid volume. Representative images of **A., E.** YAP, **B., F.** MRTF-A, **C., G.** Lamin-A and **D., H.** Vinculin stains in small (**A.-D.**) and large spheres respectively (**E.-H.**). With increasing spheroid volume there was a **I.** there was a reduction in the YAP Nuc/Cyt ratio (Pearson's correlation, $R^2 = 0.04$, $P > 0.01$, $n = 215$ spheroids, $N = 3$), **J.** a reduction in the MRTF-A Nuc/Cyt ratio (Pearson's correlation $R^2 = 0.024$, $P < 0.05$, $n = 265$ spheroids, $N = 3$), **K.** an increase in Lamin-A intensity (Pearson's correlation, $R^2 = 0.18$, $P < 0.01$, $n = 153$ spheroids, $N = 3$) and **L.** increase in Vinculin intensity (Pearson's Correlation $R^2 = 0.76$, $P < 0.01$, $n = 153$ spheroids, $N = 3$). There was no significant relationship between nuclear volume and **M.** YAP Nuc/Cyt ratio (Pearson's correlation, $R^2 = 0.01$, $P > 0.05$, $n = 215$ spheroids, $N = 3$) or **N.** MRTF-A nuc/cyt ratio (Pearson's correlation, $R^2 = 0.003$, $P > 0.05$, $n = 265$ spheroids, $N = 3$). Increasing nuclear volume was correlated with **O.** increasing Lamin-A intensity (Pearson's correlation, $R^2 = 0.41$, $p < 0.01$, $n = 271$ spheroids, $N = 3$) and **P.** Vinculin intensity increased with nuclear volume (Pearson's Correlation $R^2 = 0.49$, $P < 0.01$, $n = 153$ spheroids, $N = 3$). Values represent individual spheroids, drawn across 3 biological replicates; 'n' represents the total number of spheroids analysed.

4. Conclusion

Cell-cell interactions are known to be important for normal cardiac cell function, however, with the limited study of 3D mechanosensation of cardiac cells, the implications of these interactions have not been well explored. Our study has found that even relatively soft substrates can be a major mechanical challenge to cardiac cells in 3D but contact with other cells can enhance their capacity to respond to stiffness-based cues. In this study, we have presented a simple method for investigating collective cell mechanosensation in 3D. Many questions remain regarding how decoupling volume expansion from substrate stiffness might alter mechanotransduction and whether interactions between cardiomyocytes and common supporting cells, such as fibroblasts or endothelial cells, might enable cardiomyocytes to better adapt to 3D microenvironments. Using our platform, we have begun to unpack the mechanisms of mechanotransduction in 3D for cardiac cells, providing valuable insights for the design of cardiac structure for research and therapeutic purposes.

Author contributions

I.L.C and YS·C designed and planned the study. J.H.J and Y·H synthesized GelMA. I.L.C and S.E.A performed cell analysis. I.L.C and S.E.A drafted the manuscript. YS.C provided supervision and funding. All authors discussed the data and contributed to the final version of the manuscript. All authors have given approval to the final version of the manuscript.

Funding sources

This work was supported National Health and Medical Research Council (NHMRC) Project Grant 1098449 (to YS·C), Heart Foundation Future Leader Fellowship 101173 (to YS·C), UWA fellowship support 2018/RA/1/1997/70 (to YS·C), Future Health Research and Innovation Fund WANMA 2021 (to YS·C), NHMRC Senior Research Fellowship APP1117366 (to L.C·H), Australian Government Research Training Program Scholarship (to I.L.C and to S.E.A) and Hackett Postgraduate Research Scholarship (to S.E.A).

Declaration of competing interest

The authors declare that they have no known competing financial interests or personal relationships that could have appeared to influence the work reported in this paper.

Acknowledgements

The authors acknowledge the facilities, and the scientific and technical assistance of Microscopy Australia at the Centre for Microscopy, Characterisation & Analysis, The University of Western Australia, a facility funded by the University, State and Commonwealth Governments.

Appendix A. Supplementary data

Supplementary data to this article can be found online at https://doi.org/10.1016/j.mtbio.2022.100391.

References

[1] N.G. Frangogiannis, The extracellular matrix in ischemic and nonischemic heart failure, Circ. Res. 125 (1) (2019) 117–146.
[2] G.M. Fomovsky, J.W. Holmes, Evolution of scar structure, mechanics, and ventricular function after myocardial infarction in the rat, Am. J. Physiol. Heart Circ. Physiol. 298 (1) (2010) H221–H228.
[3] G.M. Fomovsky, A.D. Rouillard, J.W. Holmes, Regional mechanics determine collagen fiber structure in healing myocardial infarcts, J. Mol. Cell. Cardiol. 52 (5) (2012) 1083–1090.
[4] M.F. Berry, A.J. Engler, Y.J. Woo, T.J. Pirolli, L.T. Bish, V. Jayasankar, et al., Mesenchymal stem cell injection after myocardial infarction improves myocardial compliance, Am. J. Physiol. Heart Circ. Physiol. 290 (6) (2006) H2196–H2203.
[5] A. Chopra, E. Tabdanov, H. Patel, P.A. Janmey, J.Y. Kresh, Cardiac myocyte remodeling mediated by N-cadherin-dependent mechanosensing, Am. J. Physiol. Heart Circ. Physiol. 300 (4) (2011) H1252–H1266.
[6] N. Hersch, B. Wolters, G. Dreissen, R. Springer, N. Kirchgessner, R. Merkel, et al., The constant beat: cardiomyocytes adapt their forces by equal contraction upon environmental stiffening, Biol. Open 2 (3) (2013) 351–361.
[7] J.L. Young, A.J. Engler, Hydrogels with time-dependent material properties enhance cardiomyocyte differentiation in vitro, Biomaterials 32 (4) (2011) 1002–1009.
[8] J.G. Jacot, A.D. McCulloch, J.H. Omens, Substrate stiffness affects the functional maturation of neonatal rat ventricular myocytes, Biophys. J. 95 (7) (2008) 3479–3487.
[9] I.L. Chin, L. Hool, Y.S. Choi, Interrogating cardiac muscle cell mechanobiology on stiffness gradient hydrogels, Biomater. Sci. 9 (20) (2021) 6795–6806.
[10] J. Li, I. Minami, M. Shiozaki, L. Yu, S. Yajima, S. Miyagawa, et al., Human pluripotent stem cell-derived cardiac tissue-like constructs for repairing the infarcted myocardium, Stem Cell Rep. 9 (5) (2017) 1546–1559.
[11] C. Crocini, C.J. Walker, K.S. Anseth, L.A. Leinwand, Three-dimensional encapsulation of adult mouse cardiomyocytes in hydrogels with tunable stiffness, Prog. Biophys. Mol. Biol. 154 (2020) 71–79.
[12] H.K. Voges, R.J. Mills, D.A. Elliott, R.G. Parton, E.R. Porrello, J.E. Hudson, Development of a human cardiac organoid injury model reveals innate regenerative potential, Development 144 (6) (2017) 1118–1127.
[13] R.J. Mills, B.L. Parker, G.A. Quaife-Ryan, H.K. Voges, E.J. Needham, A. Bornot, et al., Drug screening in human PSC-cardiac organoids identifies pro-proliferative compounds acting via the mevalonate pathway, Cell Stem Cell 24 (6) (2019) 895–907 e6.
[14] N. Noor, A. Shapira, R. Edri, I. Gal, L. Wertheim, T. Dvir, 3D printing of personalized thick and perfusable cardiac patches and hearts, Adv. Sci. 6 (11) (2019), 1900344.
[15] M.E. Kupfer, W.H. Lin, V. Ravikumar, K. Qiu, L. Wang, L. Gao, et al., In situ expansion, differentiation, and electromechanical coupling of human cardiac muscle in a 3D bioprinted, chambered organoid, Circ. Res. 127 (2) (2020) 207–224.
[16] X. Yang, L. Pabon, C.E. Murry, Engineering adolescence: maturation of human pluripotent stem cell-derived cardiomyocytes, Circ. Res. 114 (3) (2014) 511–523.
[17] L. Polonchuk, M. Chabria, L. Badi, J.C. Hoflack, G. Figtree, M.J. Davies, et al., Cardiac spheroids as promising in vitro models to study the human heart microenvironment, Sci. Rep. 7 (1) (2017) 7005.
[18] P. Beauchamp, C.B. Jackson, L.C. Ozhathil, I. Agarkova, C.L. Galindo, D.B. Sawyer, et al., 3D Co-culture of hiPSC-derived cardiomyocytes with cardiac fibroblasts improves tissue-like features of cardiac spheroids, Front. Mol. Biosci. 7 (2020) 14.
[19] S.R. Caliari, S.L. Vega, M. Kwon, E.M. Soulas, J.A. Burdick, Dimensionality and spreading influence MSC YAP/TAZ signaling in hydrogel environments, Biomaterials 103 (2016) 314–323.
[20] H.P. Lee, R. Stowers, O. Chaudhuri, Volume expansion and TRPV4 activation regulate stem cell fate in three-dimensional microenvironments, Nat. Commun. 10 (1) (2019) 529.
[21] L.G. Major, A.W. Holle, J.L. Young, M.S. Hepburn, K. Jeong, I.L. Chin, et al., Volume Adaptation controls stem cell mechanotransduction, ACS Appl. Mater. Interfaces 11 (49) (2019) 45520–45530.
[22] O. Chaudhuri, L. Gu, D. Klumpers, M. Darnell, S.A. Bencherif, J.C. Weaver, et al., Hydrogels with tunable stress relaxation regulate stem cell fate and activity, Nat. Mater. 15 (3) (2016) 326–334.
[23] C. Kim, J.L. Young, A.W. Holle, K. Jeong, L.G. Major, J.H. Jeong, et al., Stem cell mechanosensation on gelatin methacryloyl (GelMA) stiffness gradient hydrogels, Ann. Biomed. Eng. 48 (2) (2020) 893–902.
[24] H. Kim, J.H. Jeong, M. Fendereski, H.S. Lee, D.Y. Kang, S.S. Hur, et al., Heparin-mimicking polymer-based in vitro platform recapitulates in vivo muscle atrophy phenotypes, Int. J. Mol. Sci. 22 (5) (2021).
[25] A.I. Van Den Bulcke, B. Bogdanov, N. De Rooze, E.H. Schacht, M. Cornelissen, H. Berghmans, Structural and rheological properties of methacrylamide modified gelatin hydrogels, Biomacromolecules 1 (1) (2000) 31–38.
[26] W.J. Hadden, J.L. Young, A.W. Holle, M.L. McFetridge, D.Y. Kim, P. Wijesinghe, et al., Stem cell migration and mechanotransduction on linear stiffness gradient hydrogels, Proc. Natl. Acad. Sci. U. S. A. 114 (22) (2017) 5647–5652.
[27] R. Haase, L.A. Royer, P. Steinbach, D. Schmidt, A. Dibrov, U. Schmidt, et al., CLIJ: GPU-accelerated image processing for everyone, Nat. Methods 17 (1) (2020) 5–6.
[28] R. Haase, A. Jain, S. Rigaud, D. Vorkel, P. Rajasekhar, T. Suckert, et al., Interactive design of GPU-accelerated Image Data Flow Graphs and cross-platform deployment using multi-lingual code generation, bioRxiv 11 (19) (2020), 386565.
[29] D. Legland, I. Arganda-Carreras, P. Andrey, MorphoLibJ: integrated library and plugins for mathematical morphology with ImageJ, Bioinformatics 32 (22) (2016) 3532–3534.
[30] M.S. Hepburn, P. Wijesinghe, L.G. Major, J. Li, A. Mowla, C. Astell, et al., Three-dimensional imaging of cell and extracellular matrix elasticity using quantitative micro-elastography, Biomed. Opt Express 11 (2) (2020) 867–884.
[31] S. Dupont, L. Morsut, M. Aragona, E. Enzo, S. Giulitti, M. Cordenonsi, et al., Role of YAP/TAZ in mechanotransduction, Nature 474 (7350) (2011) 179–183.
[32] H. Bian, J.Z. Lin, C. Li, S.R. Farmer, Myocardin-related transcription factor A (MRTFA) regulates the fate of bone marrow mesenchymal stem cells and its absence in mice leads to osteopenia, Mol. Metabol. 5 (10) (2016) 970–979.
[33] T. Morita, T. Mayanagi, K. Sobue, Reorganization of the actin cytoskeleton via transcriptional regulation of cytoskeletal/focal adhesion genes by myocardin-

related transcription factors (MRTFs/MAL/MKLs), Exp. Cell Res. 313 (16) (2007) 3432–3445.
[34] J. Swift, I.L. Ivanovska, A. Buxboim, T. Harada, P.C. Dingal, J. Pinter, et al., Nuclear lamin-A scales with tissue stiffness and enhances matrix-directed differentiation, Science 341 (6149) (2013), 1240104.
[35] I. Kostetskii, J. Li, Y. Xiong, R. Zhou, V.A. Ferrari, V.V. Patel, et al., Induced deletion of the N-cadherin gene in the heart leads to dissolution of the intercalated disc structure, Circ. Res. 96 (3) (2005) 346–354.
[36] D. Tirziu, F.J. Giordano, M. Simons, Cell communications in the heart, Circulation 122 (9) (2010) 928–937.
[37] J. Lammerding, P.C. Schulze, T. Takahashi, S. Kozlov, T. Sullivan, R.D. Kamm, et al., Lamin A/C deficiency causes defective nuclear mechanics and mechanotransduction, J. Clin. Invest. 113 (3) (2004) 370–378.
[38] M.H. Mokalled, K.J. Carroll, B.K. Cenik, B. Chen, N. Liu, E.N. Olson, et al., Myocardin-related transcription factors are required for cardiac development and function, Dev. Biol. 406 (2) (2015) 109–116.
[39] M.A. Trembley, P. Quijada, E. Agullo-Pascual, K.M. Tylock, M. Colpan, R.A. Dirkx Jr., et al., Mechanosensitive gene regulation by myocardin-related transcription factors is required for cardiomyocyte integrity in load-induced ventricular hypertrophy, Circulation 138 (17) (2018) 1864–1878.
[40] C. Loebel, R.L. Mauck, J.A. Burdick, Local nascent protein deposition and remodelling guide mesenchymal stromal cell mechanosensing and fate in three-dimensional hydrogels, Nat. Mater. 18 (8) (2019) 883–891.